Computers and Electronics in Agriculture 127 (2016) 109–119

Contents lists available at ScienceDirect

Computers and Electronics in Agriculture

journal homepage: www.elsevier.com/locate/compag

Original papers

Detection of dropped citrus fruit on the ground and evaluation of decay stages in varying illumination conditions

D. Choi [a], W.S. Lee [a,*], R. Ehsani [b], J. Schueller [a,c], F.M. Roka [d]

[a] Department of Agricultural and Biological Engineering, University of Florida, Gainesville, FL 32611, United States
[b] Citrus Research and Education Center, University of Florida, Lake Alfred, FL 33850, United States
[c] Department of Mechanical and Aerospace Engineering, University of Florida, Gainesville, FL 32611, United States
[d] Southwest Florida Research and Education Center, Immokalee, FL 34142, United States

ARTICLE INFO

Article history:
Received 8 December 2015
Received in revised form 4 April 2016
Accepted 31 May 2016

Keywords:
Computer vision
Contrast limited adaptive histogram equalization (CLAHE)
HLB
Outdoor imaging
Pattern recognition
Precision agriculture

ABSTRACT

The devastating disease Huanglongbing (HLB) has greatly affected citrus in Florida and other growing regions. Detecting dropped fruit is one method of estimating the presence and severity of the disease. The purpose of this study was to develop a machine vision system that can detect dropped citrus on the ground in varying illumination conditions and identify decaying stages of the dropped fruit. In this paper, a novel method for image brightness correction using a contrast limited adaptive histogram equalization was developed to produce constant image brightness levels between and within images. Objectives of this study were to: (1) solve the varying illumination problem and create a consistent brightness level between and within the images, (2) develop an algorithm to eliminate multiple detections of a single fruit from the circular Hough transform, (3) design an algorithm to evaluate decaying stages of the dropped citrus, and (4) demonstrate ability to create a fruit drop map of citrus at each decaying stage in a commercial citrus grove. The result shows all processed images had desired brightness levels (152 out of 255) with a standard deviation of 1.0. Correct identification of fruit and false positives were measured as 89.6% and 5.0%, respectively. False classifications of decay stages of fruit were as low as 4.2% and 18.5% for recently dropped fruit and rotten fruit, respectively. The techniques developed in this work could be further developed into a commercial machine vision system for a real-time dropped fruit mapping system.

1. Introduction

Citrus Huanglongbing (HLB) or citrus greening has become a devastating disease in the United States, Brazil, and other citrus-producing regions. Citrus production in the United States was estimated to 5.8 million tons in 2014–2015 crop year which was 350,000 tons lower than previous season, mainly due to the decreased production in Florida (USDA, 2015a). The widespread cases of the disease in Florida has caused production to decrease 34.4% from 189.1 million boxes in the 2008–2009 crop year to 124.0 million boxes in the 2013–2014 crop year (USDA, 2010, 2015b). There is no known cure for the disease, but it is important to know where the disease is located and the severity at those places so that mitigating actions can be taken. One approximate indicator of severity is the number of dropped fruit. However, manual inspection to find the amount of the dropped fruit increases the production costs due to labor cost (Choi et al., 2015). Using colors and shapes of citrus fruit, and the machine vision technique, the manual inspection of the dropped citrus can be automated.

However, there are common difficulties in detecting citrus fruit using outdoor images. First of all, developing an outdoor machine vision system is challenging due to varying illumination conditions among images. Many studies reported that the varying illumination caused reduced accuracy of machine vision systems for outdoor fruit detection applications (Annamalai and Lee, 2003; Annamalai et al., 2004; Stajnko et al., 2004; Patel et al., 2012; Wachs et al., 2010; Kurtulmus et al., 2011; Wang et al., 2012).

Annamalai and Lee (2003) developed a machine vision system for citrus yield mapping. However, the varying brightness levels in their images caused incorrectly detected background and missed fruit. Even though their algorithm included several processes to reduce the false positives, the system showed a performance of only $R^2 = 0.76$ between the actual number of fruit and estimated data. Wachs et al. (2010) also stated in their article that

* Corresponding author.
E-mail address: wslee@ufl.edu (W.S. Lee).

http://dx.doi.org/10.1016/j.compag.2016.05.020
0168-1699/

uncontrolled natural illumination was one of the reasons for limited performance. They developed a machine vision system using color and geometric properties to detect apples in orchards. However, the color was severely affected by unconstrained illumination. Although they combined thermal images to improve varying illumination conditions, their algorithm yielded a high false positive rate (46.8%) because their algorithm was based on the assumption that all images had the same illumination level.

Various methods were developed in many studies to overcome varying image illumination. Most of methods were based on two approaches. The first approach is to control the hardware system during image acquisition. Annamalai et al. (2004) used different shutter speeds of a camera for each image in a real-time citrus yield estimation system. They manually adjusted the shutter speed according to the light conditions. However, uneven illumination within an image was not solved by adjusting the shutter speed, and it reduced the performance during segmentation using colors. Wang et al. (2012) developed a system to evaluate the quality of cherries using their skin color. They used a flashlight with small camera aperture in order to decrease the effect of varying illumination. However, they reported that the flashlight caused highly saturated areas on fruit surfaces, and they had to use different color models for each aperture size.

The second approach to solve the varying illumination is to use software for pre-processing operations on the images. Chinchuluun and Lee (2006) adopted a gamma correction algorithm to decrease varying illumination conditions in their machine vision system for citrus yield mapping. It showed better accuracy by applying the pre-processing steps, achieving $R^2 = 0.83$ between the actual number of fruit and fruit count by the algorithm. Kurtulmus et al. (2011) developed a green citrus detection system using histogram equalization and a logarithmic transform to enhance the image brightness. Even though the image brightness was corrected, the classification algorithm showed different results depending on brightness levels of the original images. For dark images, it had a 75.2% correct identification rate and a 16.8% of false positive rate. But for the bright images, the correct identification rate was 75.4%, and the false positive rate was 40.3%. Choi et al. (2013) proposed an illumination normalization technique to develop a fruit drop detection system. The normalization was processed by dividing each RGB color component by the average gray value of all the pixels in the image. The result showed an 81.3% correct identification rate with a 12.9% false positive rate. The results from the mentioned studies show that image enhancement algorithms for preprocessing yielded better performances compared to the method controlling the hardware. The gamma correction, the logarithmic transform, and the histogram equalization are well-known methods for image enhancement. However, the main purpose of the three methods is to enhance the quality of an image. Therefore, there is no guarantee that the algorithm would reduce the differences in illumination between images. In fact, none of the above studies showed analysis about improving the consistency of image brightness between images. Therefore, in this study a pre-processing step using a contrast limited adaptive histogram equalization (CLAHE) (Zuiderveld, 1994) was introduced to have a constant image brightness level not only within an image but also between images.

The second challenge is that to keep the same distance from a camera to the fruit is difficult in an outdoor machine vision system resulting in a wide range of fruit sizes among the images. A circular Hough transform (CHT) is the commonly used method to find potential fruit areas using shape information. However, due to the wide range of the fruit sizes in the images, the CHT can cause multiple detections of a single fruit with different sizes of circles (Bansal et al., 2013; Sengupta and Lee, 2014; Silwal et al., 2014). To locate accurate fruit areas without multiple detections, Bansal et al. (2013) suggested using an average of centers of overlapped fruit. Another approach was proposed by Sengupta and Lee (2014) to select the largest radius circle among the overlapped ones. However, averaging the circles' locations or picking the largest circle disregarded the actual context within the detected areas and caused the choosing of an inappropriate circle containing not only the fruit region but also some of the background. Therefore, in this study, a new technique, applied canny edge density (ACED) algorithm, was developed with a canny edge detector and a morphological closing operation to locate the most proper fruit area considering the context of the detected circles from the CHT.

The overall goal of this study was to develop a machine vision system to estimate the amount of fruit drop in a commercial citrus grove. Specific objectives were:

1. To develop an algorithm to solve varying illumination condition and have constant image brightness throughout all acquired images.
2. To develop an algorithm to remove multiple detections of a single fruit from the circular Hough transform.
3. To develop an algorithm to evaluate decaying stages of the citrus so that citrus growers can understand when fruit dropping happened.
4. To create a fruit drop map of citrus at each decaying stage.

2. Materials and methods

2.1. Image acquisition hardware

The image acquisition hardware was developed to (1) acquire images and GPS coordinates, (2) decrease the impact of varying illumination, and (3) protect the cameras. To achieve a continuous image acquisition process, the whole system was developed to be mounted to an all-terrain vehicle (Fig. 1a, Sportsman, Polaris Industries Inc., Medina, Minnesota). Two CMOS cameras (Sony ActionCam, Tokyo, Japan) were installed under a metal shield and recorded videos while the vehicle was driving in a citrus grove. Nontransparent rubber sheets (Fig. 1a) were attached to the shield to block sunlight. To ensure enough illumination, a powerful external LED light source (3853 Lumen/m^2 at 30 cm distance) was also installed (EXO0409, Metaphase Technologies Inc., Bensalem, PA). The shield was designed to lift tree branches while the vehicle was moving forward and installed at 45 cm above the ground to minimize collisions with the tree canopy (Fig. 1b).

Fig. 2 shows the installation of the two cameras with GPS under the metal shield. Each camera had its own GPS receiver, and small areas of the metal shield on top of the receivers were replaced with acrylic panels to receive the GPS signal without interruption.

2.2. Image acquisition in a commercial citrus grove

Images were acquired on May 20 and 21, 2014 in a commercial citrus grove (Silver Strand Groves, Immokalee, Florida, Latitude: 26.366548, Longitude: −81.469557). Videos were recorded while the vehicle moved forward along tree rows with an average speed of 4.8 km/h. The field of view of the camera was 120° and the resolution of the videos was 720 by 1280. The actual size of the field of view of the camera was about 60 cm by 75 cm (0.83 mm by 0.56 mm/pixel). The frame rate was 120 frame/sec to reduce blurred images from vibration of the vehicle. An image was extracted from every 59 frames to avoid overlapped areas between images. A total of 553 images were extracted under various brightness levels. Fig. 3 shows two example images that contained various objects such as background (soil, grass, leaves and branches) and dropped oranges from the canopy with dark and bright regions. In this research, the brightness level of an image was

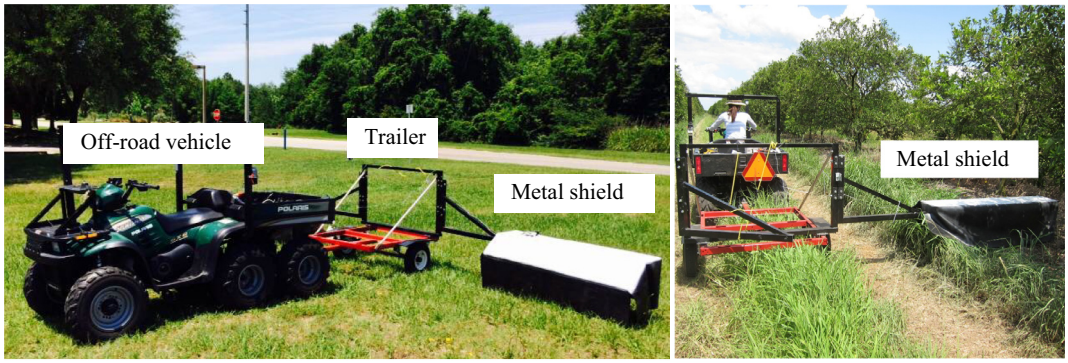

Fig. 1. Illustration of hardware setup. (a) An off-road vehicle with a metal shield and (b) illustration of image acquisition process while the vehicle was driving forward along with a tree row. The metal shield and cameras were installed at 45 cm from the ground.

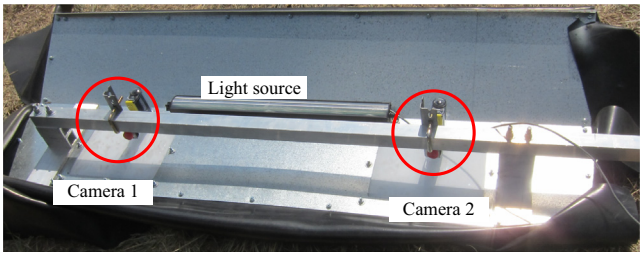

Fig. 2. Upside down picture of the shield with cameras and a light source.

defined as an average of the scaled Value (V) component (0–255) in the Hue, Saturation and Value (HSV) color space in the entire image. Two images showing different brightness levels are Fig. 3a having an average *V* component of 75.8 and Fig. 3b having an average of 100.3. The oranges in the images had largely two stages according to relative elapsed time after dropping: (1) recently dropped fruit and (2) rotten fruit.

Among the 553 images, 210 images were selected as a training set considering many possible situations including different objects and brightness levels. The other 343 images were used as a validation set. Fig. 4 illustrates a histogram of average brightness levels of all 553 training and validation images. A mean value of the brightness levels was 118.6 but varied largely among different images (standard deviation of 15.2), they ranged from 55 to 175 and were corrected in a preprocessing algorithm.

2.3. Image processing and classification algorithm

The image processing and classification algorithm was developed using Matlab (The MathWorks, Inc., Natick, Massachusetts) on a desktop computer (Intel, Core i7 3.6 GHz processor with 8 GB RAM and a 64-bit Windows 7 operating system). The algorithm consisted of image enhancement, finding fruit areas, and evaluating fruit stage into recently dropped or rotten fruit. A flowchart of the algorithm is shown in Fig. 5. Details of each step are explained in the following subsections.

2.3.1. Image preprocessing using contrast limited adaptive histogram equalization (CLAHE)

Constant brightness level is one of the key factors for good classification result for outdoor imaging since the brightness levels can critically affect color and texture of the images. Therefore, a preprocessing step using contrast limited adaptive histogram equalization (CLAHE) was implemented for post-imaging illumination correction. Originally, CLAHE was developed for improving contrast within an image, especially for medical images (Cheng et al., 2006; Morrow et al., 1992; Pisano et al., 1998; Youssif et al., 2008). The CLAHE is similar to adaptive histogram equalization (AHE). Both algorithms improved a major drawback of histogram equalization (HE), losing details due to overly contrasted areas. For example, in some cases when an image has bright and dark parts at the same time, the bright part becomes brighter, and the dark part becomes darker decreasing the overall quality of the image. Unfortunately, outdoor images often carry sunny and shadow parts together, which one of the major reasons that many global illumination correction methods would fail. On the other hand, the CLAHE and the AHE adopt a regional scheme, dividing an image into multiple sections and applying individual histogram for each section to prevent over-contrast and generate relatively uniform levels of intensities of an image regardless of illumination of original images. However, the AHE often amplifies noise in the image. The CLAHE refrains from amplifying the noise by limiting sudden increases of slopes in the cumulative probability density function of the histogram. Various

Fig. 3. Example images containing various objects and image brightness. Two images had different brightness levels: (a) average brightness of 75.8 and (b) average brightness of 100.3.

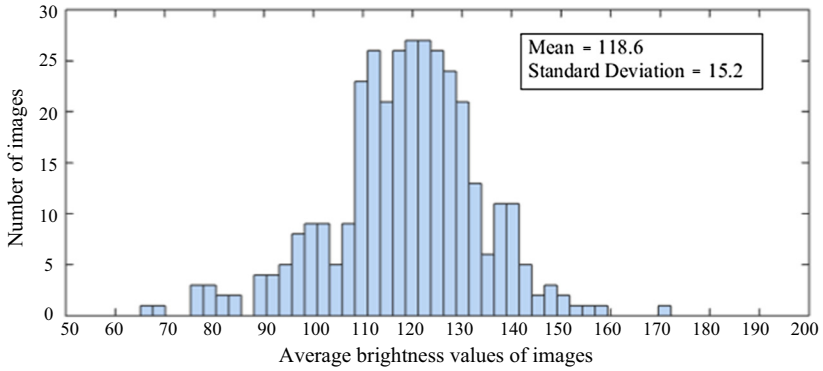

Fig. 4. Histogram of average brightness levels of the 553 images used in the research.

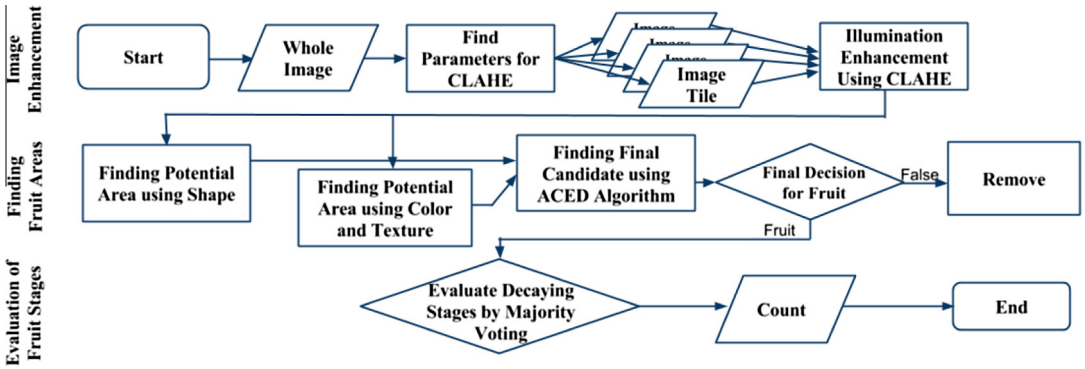

Fig. 5. Flowchart of a proposed machine vision algorithm.

forms of CLAHE can be used by a choice of redistribution functions such as uniform, exponential, and Rayleigh distributions. In this research, the main objectives of the enhancement were to correct for variable lighting conditions and to have constant brightness levels between images, and within an image. Therefore, the Rayleigh distribution function in Eq. (1) was used, since it enables adjustment of the average illumination level easier than other distribution functions by choosing different distribution function scale parameters (σ). The function is:

$$f(x,\sigma) = \frac{x}{\sigma^2} e^{-x^2/2\sigma^2}, \quad x \geqslant 0 \tag{1}$$

where x represents a random variable (the V component value of a pixel in the HSV color space in this study).

In this research, three parameters were used in the CLAHE: (1) number of tiles (n), (2) clip limit (CL) and (3) distribution scale parameter (σ). The number of tiles (n) represents how many image sections an image was divided into. A bigger number of tiles resulted in a smaller local region for which individual histogram equalization was applied. The number of tiles should be chosen carefully according to the image context; a local region should be larger than the size of objects in an image since a smaller number of tiles (bigger size of local region) may generate overly contrasted areas. The clip limit (CL) prevents amplification of noise. Since the CLAHE divides an image into small regions, and if a region had a noise, the noise would be amplified, and visibility of the noise will be enhanced. However, if too large CL value was used, it also generates overly contrasted images. Lastly, the scale (σ) of the Rayleigh distribution function is used to adjust overall levels of illumination of a region.

All images had different parameter values according to its image context. The individual heuristic search process for the three parameters was conducted for each image. Using the best first method, the most appropriate parameter values were found to have the desired illumination level (153 in scaled V component (0–255) in HSV color space). In the best first method, various candidates of parameters and corrected brightness levels using the candidate parameters were provided. The search criterion was the minimum brightness level difference with the desired brightness levels (153). This search method started from the number in a most significant digit of the parameter, and then expanded to decide numbers in smaller digits. The iteration was continued until the difference between desired brightness level and the corrected brightness level using the candidate parameters falls into the threshold, 0.01.

2.3.2. Finding potential fruit areas using shape, color, and texture

After the illumination enhancement, the algorithm searched for potential fruit areas from the background. Firstly, a circular Hough transform (CHT) was applied to find circular objects in an image. To apply the CHT at lower computation costs, image gradient of gray-level images was obtained. Since the image gradient is relatively smaller within an object than between object, pixels inside object were removed using a threshold decided from the training set. Then, the CHT was applied to find circular objects. However, due to the roughness of the ground, camera heights above the ground were not constant. This caused different sizes of objects depending on the heights of the cameras. Fig. 6 shows different sizes of fruit in the images taken at two different heights. Fig. 6a was acquired at a closer distance from the ground, and a radius of the citrus fruit in the center was about 100 pixels. On the other hand, the image of fruit in Fig. 6b was taken at further distance resulted in a smaller fruit radius (37 pixels).

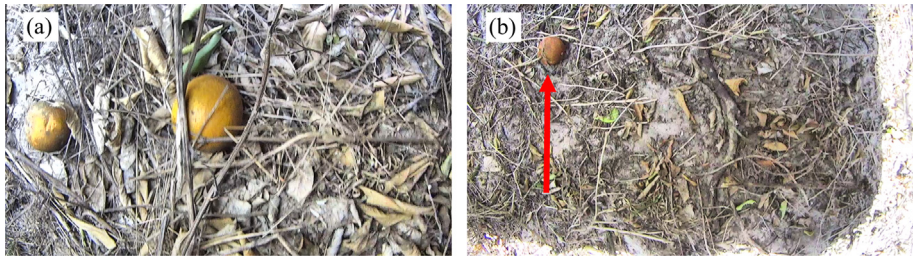

Fig. 6. Different sizes of fruits in images taken at different heights. (a) Camera at a closer distance: fruit radius of 100 pixels. (b) Camera at higher position: fruit radius of 37 pixels.

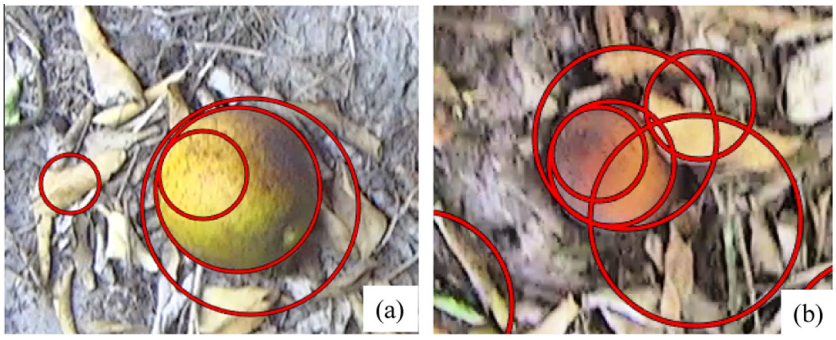

Fig. 7. Multiple detections from the CHT (red circles). (a) Multiple circles detected on a single fruit ranged from 30 to 150-pixel radius, and (b) overlapped circles containing fruit and background objects together. (For interpretation of the references to color in this figure legend, the reader is referred to the web version of this article.)

Therefore, the CHT was applied to detect circular objects with a wide range of radii. The range of radii was decided from manual inspection of the fruit sizes in the training set, and it was found to be between 30 pixels and 150 pixels. The wide range of radii in the CHT caused multiple detections of circles on an object (Fig. 7a) and other backgrounds that were overlapped with the fruit were also detected (Fig. 7b).

However, not all oranges can be detected using the CHT. Some fruits were occluded by background, and the oranges that were located at the corner of the images resulted in random shapes (red arrow in Fig. 8a). Another step to find potential fruit areas using color and texture was tested. An image was sectioned into smaller patches and a random forests (RF) classifier (Breiman, 2001) evaluated if the individual patches belonged to the fruit class using color and texture features. Different patch sizes; 10 by 10, 20 by 20 and 30 by 30 pixels was examined to find what sizes of the patch would perform better to detect fruit areas. The biggest patch size was constrained to be 30 by 30 because the smallest fruit in the training set was 30 by 30 pixels. A connected component of detected patches was added as potential fruit areas (Fig. 8b).

To train the RF classifier for potential fruit areas, 18 color and texture features were extracted from manually labeled objects in the training set. Table 1 shows the list of features that were used.

Table 1
List of features that were used in the classification step. The left column describes the features, and the right column shows numbers of features.

Description	Number of features
Red, green, and blue in RGB color space	3
Hue, saturation, and value in HSV color space	3
Luminance, chrominance in red, and chrominance in blue in YCbCr color space	3
Luminance, a, and b in Lab color space	3
Gray level	1
Gradient of gray level image	1
Edges in gray level image detected by canny method	1
Entropy of gray level image	1
Standard deviation of gray level image	1
Range of gray level image	1
Total	18

2.3.3. Choosing the most appropriate citrus-containing circle using applied canny edge density (ACED) algorithm

Detecting potential fruit areas using the CHT and the RF classifier created multiple detections of fruit with different sizes of circles (Fig. 9a). Previous studies by Bansal et al. (2013) and Sengupta and Lee (2014) addressed the same problem in their

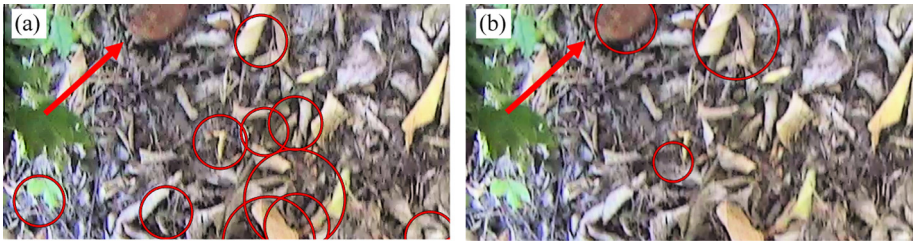

Fig. 8. Comparison of two methods to find potential areas of fruit. (a) CHT: failed to find oranges that had a weak circular shape, and (b) finding fruit using color and texture: less dependency on the fruit shape. (For interpretation of the references to colour in this figure legend, the reader is referred to the web version of this article.)

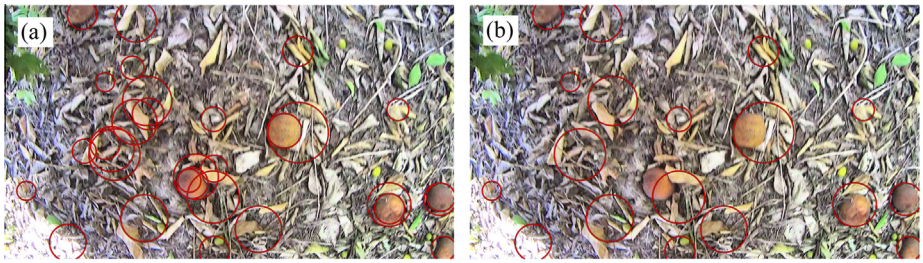

Fig. 9. Incorrectly located circles by picking the maximum size of circles among the overlapped. (a) Overlapped circles before repeated circle removal and (b) after the removal process by choosing maximum size of circles, failed to choose the most appropriate fruit area.

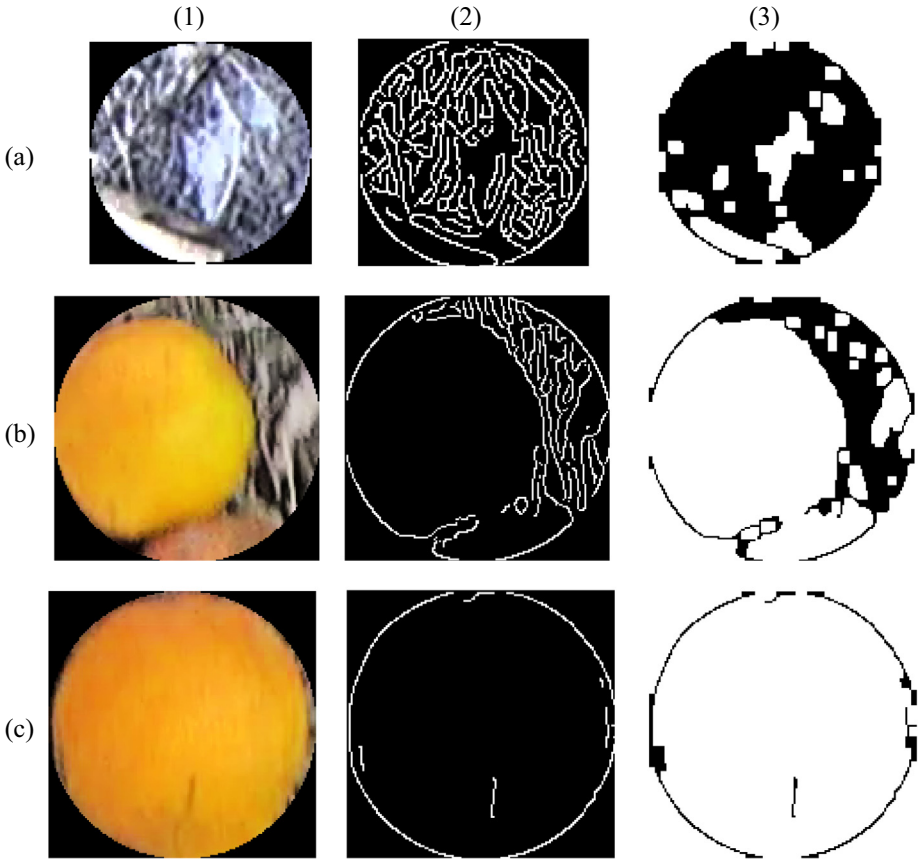

Fig. 10. Comparison of the ACED values of detected circles. RGB images of the detected circles, canny edge images, and complement images of filtered circles are shown in the first, the second, and in the last column, respectively. (a) A circle with complicated background (ACED = 0.24), (b) a circle that contained the citrus fruit and the background together (ACED = 0.76), and (c) a circle with a single fruit (ACED = 0.96).

algorithms. In their research, Bansal et al. (2013) used an average of centers of overlapped fruit, and Sengupta and Lee (2014) selected the largest radius circles among overlapped circles. However, averaging the center location or using the maximum size of circles resulted in failures in the proper selection of fruit areas (Fig. 9b).

Therefore, an applied canny edge density (ACED) algorithm was proposed to choose the most appropriate citrus-containing circles among the repeated ones. The motivation of the ACED was that circles containing more objects have more edges. A canny edge detection algorithm was used to find edges and a morphological close operation was applied with a disc-shaped filter. By the operations, regions that have more edges were filled. Other regions without edges were left as empty spaces. Then, the circle images were complemented. Densities were calculated by dividing a number of white pixels in the complemented region by area of the detected circle to be used as the ACED values. The ACED value is close to 1 when it contained a single fruit within a circle. Fig. 10 shows the process of calculating the ACED value of the detected circles. In Fig. 10, RGB images of the detected circles, canny edge images, and complement images of filtered circles are shown in the first, the second, and in the last column, respectively. Fig. 10a shows the circle that contained more than two objects (soil, dried grass and leaves) and many edges were detected. After the filtering and complementing, the most region within the circle was emptied (ACED = 0.24). Fig. 10b shows the circle that contained a fruit with some of the background objects. The ACED value in Fig. 10b is larger (0.76) than the circle in Fig. 10a since it contained fewer objects and edges. Lastly, the circle in Fig. 10c was much higher (0.96) since it contained only single fruit within the circle. All overlapped circles were removed and a circle that has the highest ACED value was chosen.

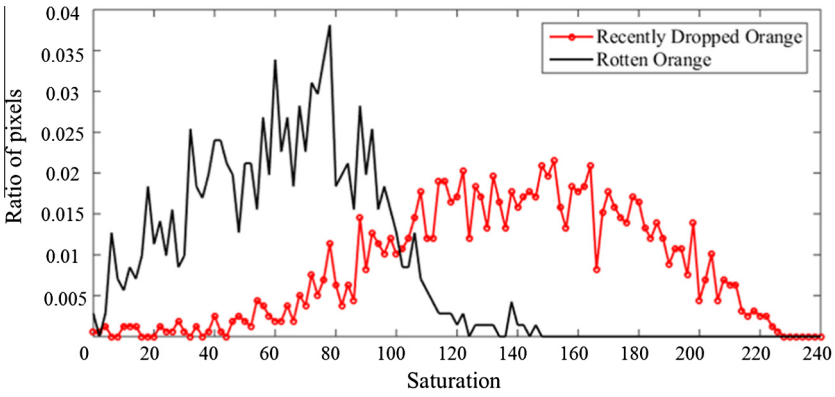

Fig. 11. Histogram of saturation values of the recently dropped fruit and rotten fruit.

Table 2
List of selected features that were used in the second classification step according to the three patch sizes.

Patch size	Number of selected features	Description of selected features
10 by 10	10	S, a, Cr, canny edge, gradient, H, entropy, B in RGB, R, and b in Lab color space
20 by 20	4	S, a, canny edge, and gradient
30 by 30	5	S, Cr, canny edge, a, and gradient

2.3.4. Evaluating decaying stages of fruit

The detected circle was then divided into smaller patches (10 by 10, 20 by 20 and 30 by 30 pixels) and classified again using another RF classifier into three categories: background, recently dropped fruit and rotten fruit. To train the second classification, saturation values in the HSV color space were used to label the two fruit stages, recently dropped fruit and rotten fruit. Fig. 11 shows the histogram of manually cropped images of the recently dropped and the rotten oranges from the 210 training images. Two histograms were intersected each other at 101, and this value was used as the threshold to divide two classes for the training images.

For feature selection, a subset of the 18 features in Table 1 was created according to the feature importance using the out-of-bag (OOB) errors in the RF (Breiman, 2001). During the training process, each tree in the RF uses only 2/3 of data, and the rest was tested to estimate the error (OOB error). Creation of a subset was started with the most important feature, and more features were added until the OOB error of the subset had less than 1% difference with the original OOB error with full features in Table 1.

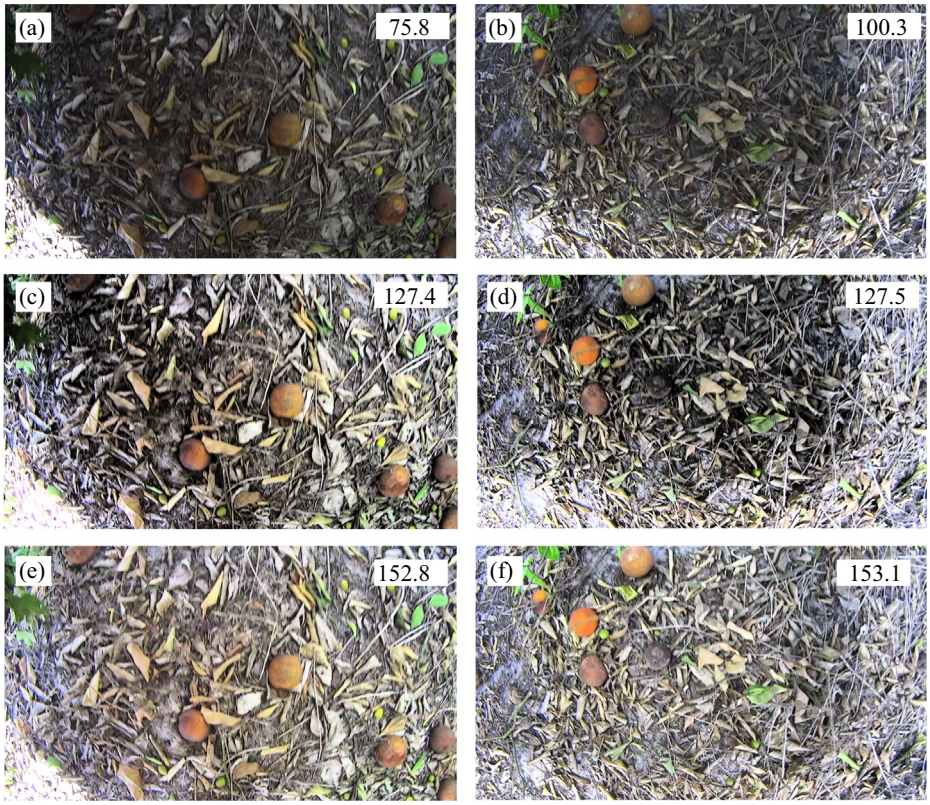

Fig. 12. Comparison of different image enhancement method: standard histogram equalization (HE) and contrast limited adaptive histogram equalization (CLAHE). Numbers on the images represent average image brightness of the images. (a) and (b) original images, (c) and (d) enhanced images using the HE, and (e) and (f) enhanced images using the CLAHE.

Table 2 shows the list of selected features for the different patch sizes. A total of ten, four, and five features were selected for the 10 by 10, 20 by 20, and 30 by 30 patch size, respectively. Then, a majority voting was conducted for the final class decision. If the fruit areas did not exceed 50% of the entire region, the circle was classified as the background. Non-background circles were selected based upon calculated percentages of rotten fruit areas to estimate the stages of the detected fruit. After the estimation of the stages of the detected fruit, the number of the recently dropped fruit and the rotten fruit were counted. The results were combined with GPS coordinates to create a geo-referenced fruit drop map. Two volunteers participated in evaluating results of the algorithm. The volunteers identified the numbers of actual fruits, missed fruits (fruit not detected by the algorithm), correctly identified fruit, and false positives (backgrounds detected as the citrus by the algorithm) in the images. The fruit stage classification (the recently dropped, and the rotten fruits) was then evaluated among the correctly identified fruit. The average of saturation value was calculated and compared with the threshold decided in Fig. 11. The fruits that did not meet the threshold were counted as the false classification of the stages.

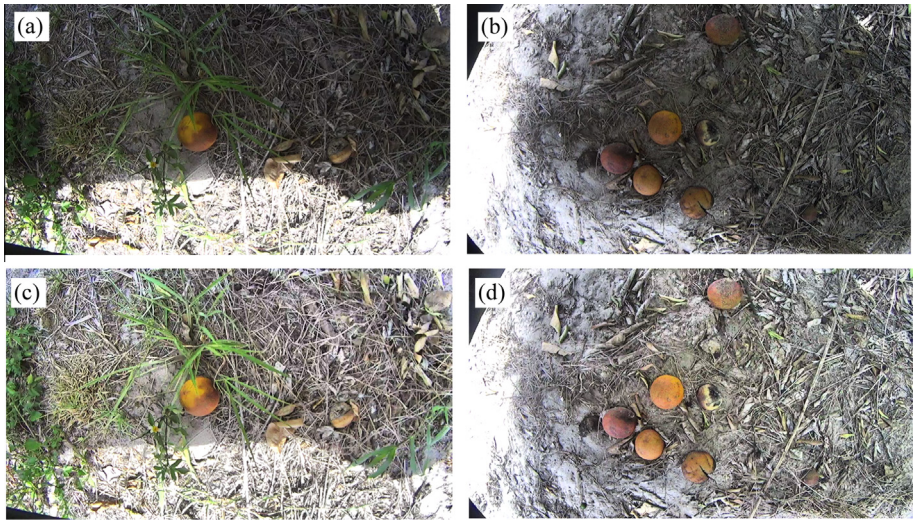

Fig. 13. Additional examples of the CLAHE enhancement for images that had more brightness gaps within the images. (a) and (b) original images and (c) and (d) enhanced images using the CLAHE.

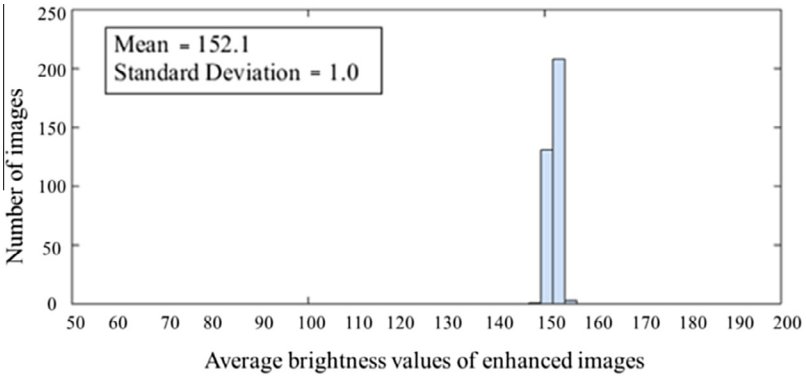

Fig. 14. Histogram of average brightness levels in enhanced images. All images had the constant brightness near to 152.

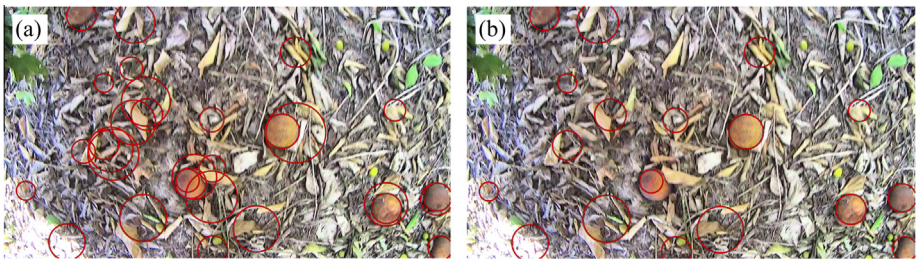

Fig. 15. Illustration of finding potential areas. (a) multiple detection of a single fruit after the CHT and the RF classifier and (b) circle removing process using the ACED values.

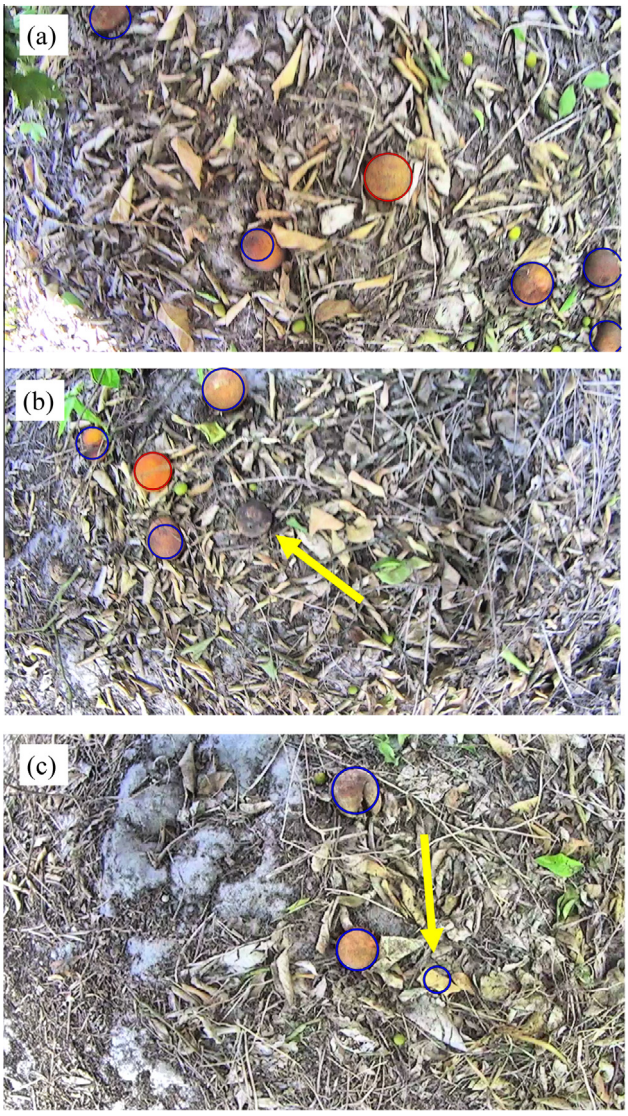

Fig. 16. Example images from final classification result of the fruit stages (red circle: recently dropped fruit, and blue circle: rotten fruit). (a) Correctly identified fruits, (b) missed fruit in the center due to the similarity with the background, and (c) false positive of the leaves due to the similarity of the color with the citrus. (For interpretation of the references to colour in this figure legend, the reader is referred to the web version of this article.)

3. Results and discussion

3.1. Result of image enhancement using CLAHE

Fig. 12 shows a comparison of original images (Fig. 12a and b), enhanced images using the standard histogram equalization (Fig. 12c and d), and enhanced images using the CLAHE (Fig. 12e and f). Average brightness levels of the original images were in different ranges, 75.8 and 100.3. After the image enhancement using the HE, the brightness levels became similar, about 127 for both images. However, the center of the images was excessively contrasted, changing many pixels to a darker color. The enhanced images using the CLAHE (Fig. 12e and f) restrained the over-contrasting, and the images preserved its details. The average brightness levels were adjusted to have a brighter and desired level (153 in scaled value component in HSV), which was not possible when using the standard HE. Also, Fig. 13 shows that the CLAHE was able to enhance the images that had bigger gaps in brightness levels between dark and bright regions.

Enhanced images of all 553 images, including the training and validation sets, had the constant brightness levels around 152 with a standard deviation of 1.0. Fig. 14 shows a distribution of average brightness levels after the enhancement. Compared to the distribution of original images in Fig. 4, brightness levels of the images were greatly improved and had almost the same brightness values.

3.2. Result of finding potential fruit areas using shape, color and texture

The potential fruit areas were detected using the CHT and the RF classifier with color and texture (Fig. 15a). In the image in Fig. 15a, the fruits are detected multiple times, and some of the detected areas included backgrounds. The repeatedly detected circles were removed, and the circle that had the highest ACED value remained. Fig. 15b shows that the circles were chosen correctly without containing other background objects.

After the circle removal, the second classification by patch using the RF was conducted within the detected circles. The background objects were identified during this process. Also, the stages of dropped fruit were decided by the majority voting. Fig. 16 shows final decision by majority voting. Red circles represent recently dropped citrus, and blue circles represent rotten ones. Most of the fruit were detected correctly. However in Fig. 16b, the fruit in the center was not detected due to the similarity of color and texture with background. Fig. 16c shows an example of false positive; a leaf was detected as a citrus due to the similarity of the color and texture with the citrus. Table 3 shows a summary of results from fruit detection algorithm validated by two volunteers. The highest average rate of correctly identified fruit was 94.6% when the patch size was 10 by 10. However, the classifier with the 10 by 10 patch size generated the highest rate of false positives since the patch was too small to capture the texture of the fruit properly. On the other hand, a 30 by 30 patch was larger than the minimum size of the smallest fruit resulting in many missed fruits. Considering both the false positives and the correctly identified fruit rates together, it was concluded that the 20 by 20 patch (1.7 cm by 1.2 cm) was the most appropriate size for the fruit detection application. In a previous study for detecting citrus fruit drop using outdoor RGB images, Choi et al. (2015) reported 88.1% of the correctly identified fruit. Compared to the previous article, this study showed improved performance to detect dropped fruits.

Table 3
Result of fruit detection rate by the number of correctly identified fruit and false positives.

Actual number of fruit		Manual counting 1: 926		Manual counting 2: 947		Average: 936.5	
Patch size	Count by algorithm	Correctly identified fruit (%)	False positives (%)	Correctly identified fruit (%)	False positives (%)	Correctly identified fruit (%)	False positives (%)
10 by 10	1032	876 (94.6)	156 (16.8)	885 (93.5)	147 (15.5)	880.5 (94.0)	151.5 (16.2)
20 by 20	886	836 (90.3)	50 (5.4)	843 (89.0)	43 (4.5)	839.5 (89.6)	46.5 (5.0)
30 by 30	786	759 (82.0)	27 (2.9)	764 (80.7)	22 (2.3)	761.5 (81.3)	24.5 (2.6)

3.3. Result of evaluating stages of fruit using random forest classifier

Among the correctly identified fruits, the result of evaluating stages of the citrus, the recently dropped and rotten fruit were validated by comparing the result from the classifier and the majority voting with the classes decided from the threshold in Fig. 11. Table 4 shows the false classification rates of fruit stages which was calculated by dividing the number of the falsely classified stages by the actual number of each class. The lowest false classification rates for the recently dropped fruit was 4.2% when the patch size was 30 by 30. Since the stages of the dropped fruits were validated using the average of saturation values so the bigger size of patch performed more effectively. However, the false positive rate of the rotten fruit was lowest when the 10 by 10 patch was used (18.5%). For the rotten fruit, most of the fruit had non-uniform surface including the color and texture, partly with blemish and different colors. Therefore, the smaller size of the 10 by 10 patch evaluated the rotten fruits more accurately. Due to the uniqueness of the topic, there are not enough published studies related to citrus stage evaluation using outdoor RGB images. However, Fadilah et al. (2012) reported 91.6% accuracy to evaluate ripeness of oil palm fresh fruit using outdoor RGB images. However, an image contained only one fruit and the size of fruit was filled entire of an image. Also, the images did not involve varying illumination conditions. Considering those circumstances, the result from this study had meaningful achievement.

The counts of both stages of the fruit were combined with GPS coordinates to generate a geo-referenced map. Fig. 17 shows example maps created utilizing a satellite image from Google Earth. Using the fruit drop map, citrus growers can visualize where, and when the citrus fruit dropping is the most prevalent in their groves and provide block specific management to have better fertilization and irrigation of the areas.

Table 4
Result of evaluating stages of fruit. Each column in manual counting 1&2 and its average represents false classification rate of each classes: recently dropped fruit and rotten fruit.

Patch size	Manual counting 1				Manual counting 2			
	Recently dropped fruit		Rotten fruit		Recently dropped fruit		Rotten fruit	
	Actual no.	False positives (%)	Actual no.	False positives (%)	Actual no.	False positives (%)	Actual no.	False positives (%)
10 by 10	449	18 (4.0)	427	82 (19.2)	451	20 (4.4)	434	77 (17.7)
20 by 20	442	22 (5.0)	394	80 (20.3)	443	24 (5.4)	400	76 (19)
30 by 30	439	10 (2.3)	320	107 (33.4)	438	11 (2.5)	326	102 (31.2)
	Average							
	Recently dropped fruit		Rotten fruit					
	Actual no.	False positives (%)	Actual no.	False positives (%)				
10 by 10	450	19 (4.2)	430.5	79.5 (18.5)				
20 by 20	442.5	23 (5.2)	397	78 (19.6)				
30 by 30	438.5	10.5 (2.4)	323	104.5 (32.3)				

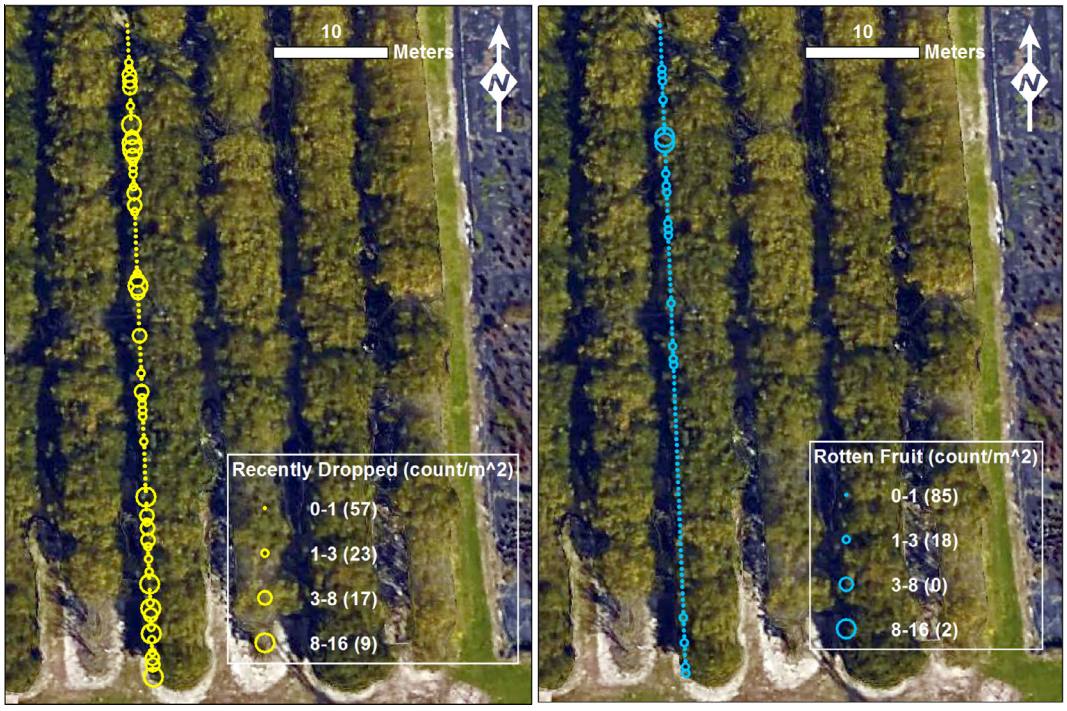

Fig. 17. Example of geo-referenced maps utilizing a satellite image. Number in parenthesis in legend represent the number of events in each category. The map was created using additional field experiment in University of Florida experimental grove (Gainesville, Florida) conducted on April 25, 2014.

4. Conclusion

A machine vision system was developed for counting dropped citrus fruit under tree canopies and evaluating its stages: recently dropped fruit or rotten fruit. The contrast limited adaptive histogram equalization (CLAHE) enhanced the brightness of all images to have the constant image brightness levels. The proposed algorithm improved accuracy of the classification compared to previous studies. The performance of fruit detection algorithm was the highest (89.6% for correct identification and 5.0% for false positive rates) when the patch size was 20 by 20 (1.7 cm by 1.2 cm). This shows that a choice of an appropriate patch size is an important task, the patch should be large enough to contain texture information but not exceed the size of the fruit. However, the classification of fruit stages showed different patch sizes performed better depending on the features of each stages. By estimating citrus fruit drop and creating a fruit drop map, block specific management can be achieved to provide better fertilization and irrigation programs that can help to treat the HLB-infected trees in order to delay tree death and prevent infection within a tree (Salifu et al., 2013). The machine vision system demonstrated here could be further developed into a real-time system for use in commercial citrus groves.

Acknowledgement

This project was supported by the University of Florida/Institute of Food and Agricultural Sciences' Citrus Initiative program. The authors would like to thank Mr. Michael Zingaro, Dr. Alireza Pourreza, Dr. Mazin Saber, Ms. Mubarkat Shuaibu and Ms. Brianna Posadas at the University of Florida for their assistance with this research.

References

Annamalai, P., Lee, W.S., 2003. Citrus yield mapping system using machine vision. In: Paper Presented at the 2003 ASAE Annual Meeting.

Annamalai, P., Lee, W.S., Burks, T.F., 2004. Color vision system for estimating citrus yield in real-time. In: Paper Presented at the 2004 ASAE Annual Meeting.

Bansal, R., Lee, W.S., Satish, S., 2013. Green citrus detection using fast Fourier transform (FFT) leakage. Precis. Agric. 14 (1), 59–70. http://dx.doi.org/10.1007/s11119-012-9292-3.

Breiman, L., 2001. Random forests. Mach. Learn. 45 (1), 5–32. http://dx.doi.org/10.1023/a:1010933404324.

Cheng, H.D., Shi, X.J., Min, R., Hu, L.M., Cai, X.R., Du, H.N., 2006. Approaches for automated detection and classification of masses in mammograms. Pattern Recogn. 39 (4), 646–668. http://dx.doi.org/10.1016/j.patcog.2005.07.006.

Chinchuluun, R., Lee, W.S., 2006. Citrus yield mapping system in natural outdoor scenes using the watershed transform. In: ASABE Paper (063010).

Choi, D., Lee, W., Ehsani, R., 2013. Detecting and counting citrus fruit on the ground using machine vision. In: Paper Presented at the 2013 Kansas City, Missouri, July 21–July 24, 2013.

Choi, D., Lee, W.S., Ehsani, R., Roka, F.M., 2015. A machine vision system for quantification of citrus fruit dropped on the ground under the canopy. Trans. ASABE 58 (4), 933–946.

Fadilah, N., Mohamad-Saleh, J., Abdul Halim, Z., Ibrahim, H., Syed Ali, S.S., 2012. Intelligent color vision system for ripeness classification of oil palm fresh fruit bunch. Sensors 12 (10), 14179–14195.

Kurtulmus, F., Lee, W.S., Vardar, A., 2011. Green citrus detection using 'eigenfruit', color and circular Gabor texture features under natural outdoor conditions. Comput. Electron. Agric. 78 (2), 140–149. http://dx.doi.org/10.1016/j.compag.2011.07.001.

Morrow, W.M., Paranjape, R.B., Rangayyan, R.M., Desautels, J.E.L., 1992. Region-based contrast enhancement of mammograms. IEEE Trans. Med. Imag. 11 (3), 392–406. http://dx.doi.org/10.1109/42.158944.

Patel, H., Jain, R., Joshi, M., 2012. Automatic segmentation and yield measurement of fruit using shape analysis. Int. J. Comput. Appl. 45 (7), 19–24.

Pisano, E.D., Zong, S.Q., Hemminger, B.M., DeLuca, M., Johnston, R.E., Muller, K., Pizer, S.M., 1998. Contrast limited adaptive histogram equalization image processing to improve the detection of simulated spiculations in dense mammograms. J. Digit. Imag. 11 (4), 193–200.

Salifu, A.W., Spreen, T.H., Grogan, K.A., Roka, F.M., 2013. Management of HLB infected citrus groves in Florida: some empirical results. In: Paper Presented at the 2013 Annual Meeting, February 2–5, 2013, Orlando, Florida.

Sengupta, S., Lee, W.S., 2014. Identification and determination of the number of immature green citrus fruit in a canopy under different ambient light conditions. Biosyst. Eng. 117, 51–61. http://dx.doi.org/10.1016/j.biosystemseng.2013.07.007.

Silwal, A., Gongal, A., Karkee, M., 2014. Identification of red apples in field environment with over the row machine vision system. Agric. Eng. Int.: CIGR J. 16 (4), 66–75.

Stajnko, D., Lakota, M., Hoevar, M., 2004. Estimation of number and diameter of apple fruits in an orchard during the growing season by thermal imaging. Comput. Electron. Agric. 42 (1), 31–42. http://dx.doi.org/10.1016/S0168-1699(03)00086-3.

USDA, 2010. Florida citrus statistics 2008–2009. Retrieved 2015-12-03 from <http://www.nass.usda.gov/Statistics_by_State/Florida/Publications/Citrus/fcs/2008-09/fcs0809all.pdf>.

USDA, 2015a. Citrus: world markets and trade. Retrieved 2015-12-03 from <http://apps.fas.usda.gov/psdonline/circulars/citrus.pdf>.

USDA, 2015b. Florida citrus statistics 2013–2014. Retrieved 2015-12-03 from <http://www.nass.usda.gov/Statistics_by_State/Florida/Publications/Citrus/fcs/2013-14/fcs1314.pdf>.

Wachs, J.P., Stern, H.I., Burks, T., Alchanatis, V., 2010. Low and high-level visual feature-based apple detection from multi-modal images. Precis. Agric. 11 (6), 717–735. http://dx.doi.org/10.1007/s11119-010-9198-x.

Wang, Q., Wang, H., Xie, L.J., Zhang, Q., 2012. Outdoor color rating of sweet cherries using computer vision. Comput. Electron. Agric. 87, 113–120. http://dx.doi.org/10.1016/j.compag.2012.05.010.

Youssif, A.A.-H.A.-R., Ghalwash, A.Z., Ghoneim, A.A.S.A.-R., 2008. Optic disc detection from normalized digital fundus images by means of a vessels' direction matched filter. IEEE Trans. Med. Imag. 27 (1), 11–18. http://dx.doi.org/10.1109/tmi.2007.900326.

Zuiderveld, K., 1994. Contrast limited adaptive histogram equalization. In: Paper Presented at the Graphics Gems IV, San Diego.